Bubble interaction model for hydrodynamic unstable mixing

Sung-Ik Sohn*
Department of Mathematics, Kangnung National University, Kangnung 210-702, Korea
(Received 2 January 2007; revised manuscript received 30 May 2007; published 25 June 2007)

The analytic model for the evolution of single and multiple bubbles in Rayleigh-Taylor mixing is presented for the system of arbitrary density ratio. The model is the extension of Zufiria's potential theory, which is based on the velocity potential with point sources. We present solutions for a single bubble, at various stages, from the model and show that the solutions for the bubble velocity and curvature are in good agreement with numerical results. We demonstrate the evolution of multiple bubbles for finite density contrast and investigate dynamics of bubble competition, whereby leading bubbles grow in size at the expense of neighbors. The model shows that the growth coefficient α for the scaling law of the bubble front depends on the Atwood number and increases logarithmically with the initial perturbation amplitude. It is also found that the aspect ratio of the bubble size to the bubble height exhibits a self-similar behavior in the bubble competition process, and its values are insensitive to the Atwood number. The predictions of the model for the similarity parameters are in accordance with experimental and numerical results.

DOI: 10.1103/PhysRevE.75.066312 PACS number(s): 47.20.Ma, 47.20.Ky

I. INTRODUCTION

Fluid mixing occurs frequently in basic science and engineering applications. When a heavy fluid is supported by a lighter fluid in a gravitational field, the interface between the fluids is unstable under small disturbances. This phenomenon is known as the Rayleigh-Taylor (RT) instability [1–3]. The RT instability may occur whenever the density and pressure gradients are in opposite directions and plays important roles in many fields ranging from astrophysics to inertial confinement fusion [4]. Since Rayleigh [1] first considered this problem, it has received attention in a wide range of contexts, but many aspects of dynamics of the instability are still uncertain. For a review, see Sharp [4] and Zabusky [5].

Small perturbations at the interface in the RT instability grow into nonlinear structures in the form of bubbles and spikes. A bubble (spike) is a portion of the light (heavy) fluid penetrating into the heavy (light) fluid. In a system of single-mode periodicity, the bubble attains a constant asymptotic growth rate. When the interface has multimode or random initial perturbations, different frequencies excite nonlinear interactions and the flow develops into a turbulent mixing.

The main purpose of this paper is to develop a model for single and multiple bubbles of arbitrary density ratio and present solutions for bubble evolutions. Theoretical models for comprehensive descriptions of the motion of bubbles are potential flow models proposed by Layzer [6] and Zufiria [7]. Both Layzer and Zufiria models approximate the shape of the interface near the bubble tip as a parabola and give a set of ordinary differential equations to determine the position, velocity, and curvature of the bubble. The main difference of two models is that the velocity, potential in the Layzer model is an analytical function of sinusoidal form, while in the Zufiria model, it has a point source (singularity). The Layzer and Zufiria models were limited to the case of infinite density ratio (fluid and vacuum) for a long time, but recently there has been significant progress in two models and been generalized to the system of finite density ratios for a single bubble [8–12]. Systematic comparisons of potential flow models for two-fluid systems are found in Ref. [13]. In this paper, we present solutions for a single bubble from the Zufiria model, separating stages into linear, asymptotic, and finite times, and extend the single bubble model to multiple bubbles of finite density ratio.

We will show that the Zufiria model provides good predictions for both the bubble velocity and the bubble curvature. The bubble curvature is an important parameter because it sets a length scale and plays a key role in the dynamics of the bubble interaction. The previous theoretical models for the RT instability failed to give good predictions for the bubble curvature.

The evolution of unstable interfaces with initial random perturbations are much more complicated than that of single mode. At the random perturbations, bubbles of different radii propagate with different velocities and the leading bubbles grow in size at the expense of their neighboring bubbles. This phenomenon is known as a bubble interaction or bubble merger process [4,6]. We demonstrate the evolution of multiple bubbles and investigate the dynamics of bubble interactions in the system of finite density ratios.

A central issue in the turbulent mixing by the RT instability is a scaling law for the growth of the mixing zone. It has been known that the bubble front in the RT mixing grows as

$$h = \alpha \frac{\rho_1 - \rho_2}{\rho_1 + \rho_2} g t^2, \tag{1}$$

and the coefficient α is insensitive to the density ratio [14–16], where ρ_1 and ρ_2 are the densities of heavy and light fluids, and g is a gravitation acceleration. The implication of Eq. (1) is that, at self-similarity, all memory of initial conditions are lost and the only relevant length scale is gt^2.

Several theoretical models [17–24] have been proposed to estimate the growth coefficient α, but most of them are based on statistical or phenomenological equations, which usually include unknown parameters. Contrasting to statistical and phenomenological models, our model is mathematically de-

*sohnsi@kangnung.ac.kr

rived by the potential theory and gives analytic equations to determine the bubble fronts. It will be shown that the prediction for the coefficient α from our model agrees well with the results of numerical simulations and experiments. We investigate the dependence of the growth constant α on the density ratio and initial conditions, as well as the self-similarity parameter β, defined as the ratio of the bubble size to the bubble height.

In Sec. II, we describe the potential flow model with a source singularity for the motion of a single bubble of arbitrary density ratio. In Sec. III, we present the linear, asymptotic, and finite time solutions from the potential flow model for the growth of a single bubble in RT instability and give the validation study for the solutions. In Sec. IV, the potential flow model is extended to multiple bubbles of arbitrary density ratio and, in Sec. V, it is applied to the simulation of the bubble interaction process. Section VI gives conclusions.

II. SINGLE BUBBLE MODEL

We consider an interface, in a vertical channel, between two fluids of different densities in two dimensions. The upper fluid is heavier than the lower fluid, i.e., $\rho_1 > \rho_2$. We assume that the fluids are incompressible, inviscid, and irrotational. Then, there exist complex potentials $W_1(z)=\phi_1+i\psi_1$ and $W_2(z)=\phi_2+i\psi_2$ for each fluid, where ϕ is the velocity potential and ψ the stream function. The location of the bubble tip is $Z(t)=X(t)+iY(t)$, in the laboratory frame of reference, with $Y(t)=L/2$, where L is a channel width. The bubble moves in the x direction with the tip velocity U. It is convenient to choose a frame of reference $(\hat{x},\hat{y})$ comoving with the tip of the bubble. In this moving frame, the interface around the bubble tip is approximated as

$$\eta(\hat{x},\hat{y},t) = \hat{y}^2 + 2R(t)\hat{x} = 0, \tag{2}$$

where R is the local radius of curvature.

Extending Zufiria's model [7], we take the complex potentials

$$W_1(\hat{z}) = Q_1 \ln[1 - e^{-k(\hat{z}+H)}] - U\hat{z}, \tag{3}$$

$$W_2(\hat{z}) = Q_2 \ln[1 - e^{-k(\hat{z}-H)}] + (K-U)\hat{z}, \tag{4}$$

where $k=2\pi/L$ is the wave number. The potential W_1 describes the source flow of strength Q_1, located at $(\hat{x},\hat{y})=(-H,0)$, in the uniform stream U. The potential W_2 gives the source flow of strength Q_2, located at $(\hat{x},\hat{y})=(H,0)$, in the uniform stream $U-K$. The potentials (3) and (4) can be derived from the Schwartz-Christoffel transformation [25]. The corresponding velocity potentials and the stream functions are given by

$$\phi_1 = \frac{Q_1}{2} \ln[\cosh k(\hat{x}+H) - \cos k\hat{y}] - \left(\frac{k}{2}Q_1 + U\right)\hat{x}, \tag{5}$$

$$\psi_1 = Q_1 \arctan\left(\coth\frac{k(\hat{x}+H)}{2}\tan\frac{k\hat{y}}{2}\right) - \left(\frac{k}{2}Q_1 + U\right)\hat{y}, \tag{6}$$

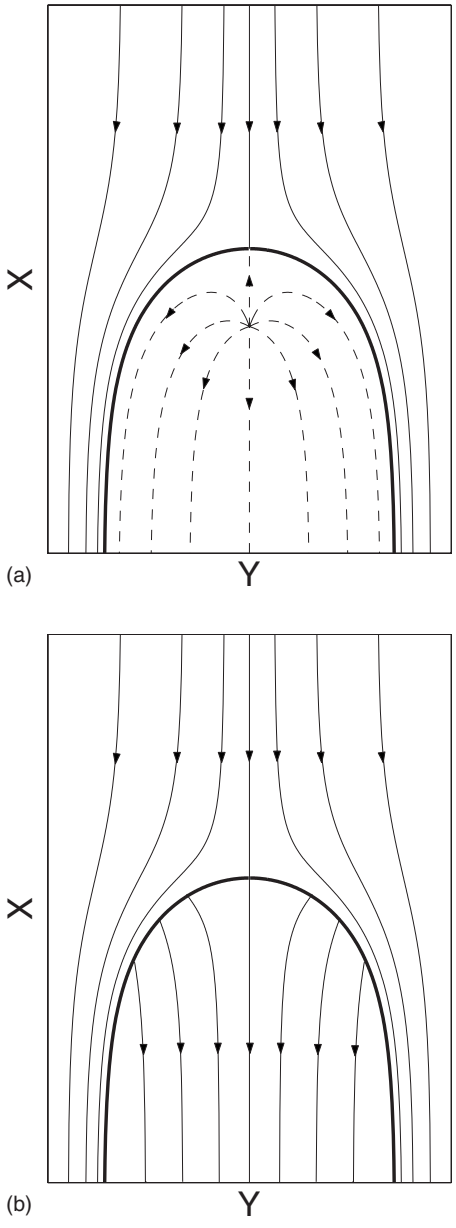

FIG. 1. Streamline pattern. (a) Streamlines of ψ_1. (b) Streamlines of ψ_1 and ψ_2.

$$\phi_2 = \phi_1(Q_1 \to Q_2, H \to -H, U \to U-K), \tag{7}$$

$$\psi_2 = \psi_1(Q_1 \to Q_2, H \to -H, U \to U-K). \tag{8}$$

We consider the streamline pattern of ψ_1 and ψ_2. The streamline through an arbitrary reference point $(\hat{x_0},\hat{y_0})$ is defined by $\psi_i(\hat{x},\hat{y})=\psi_i(\hat{x_0},\hat{y_0})$, $i=1,2$. Figure 1(a) illustrates the streamlines of ψ_1, which correspond to the infinite density ratio case. The curve obtained by the streamline $\psi_1(\hat{x},\hat{y})=\psi_1(0,0)$ through the stagnation point at $\hat{x}=\hat{y}=0$ determines the bubble profile. In fact, the streamlines of ψ_1 below the bubble profile are artificial, because the potential W_1 serves the flow of the upper fluid. Figure 1(b) shows the streamlines of ψ_1 and ψ_2, which describe the flow of a bubble of finite density contrast. The streamlines of ψ_2 can be obtained by

flipping those of ψ_1 with respect to the line $\hat{x}=0$ and taking only the curves below the bubble profile.

From the relation $\psi_1(\hat{x},\hat{y})=\psi_1(0,0)$, we find that the analytic expression of the bubble profile is

$$\hat{x}=\frac{1}{k}\ln\left[\frac{\sin(\gamma k\hat{y})}{\sin(\delta\gamma k\hat{y})}\right]-H, \tag{9}$$

where $\delta=e^{-kH}$ and $\gamma=1/(1-\delta)$. Expanding this equation at $\hat{y}=0$, the radius of the bubble curvature is given by

$$R=\frac{3(e^{kH}-1)}{k(e^{kH}+1)}. \tag{10}$$

This equation provides the relation between the variables R and H. We see that, for $H>0$, the dimensionless curvature $1/(kR)$ is larger than $1/3$. This fact implies that the present model is valid, in a strict sense, for moderately small initial amplitudes, and does not give early time solutions of bubble evolutions with very small initial amplitudes. The bubble width also can be obtained from Eq. (9). Setting $\sin(\gamma k\hat{y})=0$ in Eq. (9), one finds the bubble width λ by

$$\lambda=(1-e^{-kH})L. \tag{11}$$

The evolution of the bubble is determined by the kinematic condition and the Bernoulli equation

$$\frac{D\eta(\hat{x},\hat{y},t)}{Dt}=2\frac{dR}{dt}\hat{x}+2Ru_i+2\hat{y}v_i=0, \quad \text{for } i=1,2, \tag{12}$$

$$\rho_1\left[\frac{\partial\phi_1}{\partial t}+\frac{1}{2}(\nabla\phi_1)^2+\left(g+\frac{dU}{dt}\right)\hat{x}\right]=\rho_2\left[\frac{\partial\phi_2}{\partial t}+\frac{1}{2}(\nabla\phi_2)^2+\left(g+\frac{dU}{dt}\right)\hat{x}\right], \tag{13}$$

where u_i and v_i, $i=1,2$, are $\hat{x}$ and $\hat{y}$ components of the interface velocity taken from the upper and lower fluids. The kinematic condition implies the continuity of the normal component of fluid velocity across the interface.

Expanding the complex potentials (3) and (4) in powers of $\hat{z}$, we have

$$W_1=Q_1\sum_{n=0}^{\infty}\frac{c_n}{n!}\hat{z}^n-U\hat{z}, \tag{14}$$

$$W_2=Q_2\sum_{n=0}^{\infty}\frac{\tilde{c}_n}{n!}\hat{z}^n+(K-U)\hat{z}. \tag{15}$$

It is easy to check that $c_{n+1}=dc_n(H)/dH$ and $\tilde{c}_{n+1}=-d\tilde{c}_n(H)/dH$ for $n\geq 0$, with $c_0=\ln(1-e^{-kH})$ and $\tilde{c}_0=\ln(1-e^{kH})$.

The relations $dW_i/d\hat{z}=u_i-iv_i$, $i=1,2$, give the expressions for the interface velocity

$$u_1=Q_1[c_1+(c_2+c_3R)\hat{x}]-U+O(\hat{x}^2),\qquad v_1=-c_2Q_1\hat{y}+O(\hat{x}^{3/2}), \tag{16}$$

$$u_2=Q_2[\tilde{c}_1+(\tilde{c}_2+\tilde{c}_3R)\hat{x}]+(K-U)+O(\hat{x}^2),\qquad v_2=-\tilde{c}_2Q_2\hat{y}+O(\hat{x}^{3/2}). \tag{17}$$

Substituting Eqs. (16) and (17) into the kinematic condition (12) and satisfying up to first order in $\hat{x}$, it gives

$$\frac{dX}{dt}=U=c_1Q_1=\tilde{c}_1Q_2+K, \tag{18}$$

$$\frac{dR}{dt}=-Q_1(3c_2+c_3R)R=-Q_2(3\tilde{c}_2+\tilde{c}_3R)R. \tag{19}$$

In fact, in the present model, the kinematic condition (12) is satisfied for all values of $\hat{x}$. One can check the satisfaction of the kinematic condition for higher order in $\hat{x}$, expanding the approximations of the interface (2), and fluid velocities (16) and (17), to higher order.

Using Eqs. (14) and (15), the first and second order equations in $\hat{x}$ of Eq. (13) are

$$(c_1+c_2R)\frac{dQ_1}{dt}+Q_1(c_2+c_3R)\frac{dH}{dt}-Q_1^2c_2^2R+g=\mu\left[(\tilde{c}_1+\tilde{c}_2R)\frac{dQ_2}{dt}+\frac{dK}{dt}-Q_2(\tilde{c}_2+\tilde{c}_3R)\frac{dH}{dt}-Q_2^2\tilde{c}_2^2R+g\right], \tag{20}$$

$$\left(\frac{c_2}{2}+c_3R+c_4\frac{R^2}{6}\right)\frac{dQ_1}{dt}+Q_1\left(\frac{c_3}{2}+c_4R+c_5\frac{R^2}{6}\right)\frac{dH}{dt}+\frac{1}{2}F_1=\mu\left[\left(\frac{\tilde{c}_2}{2}+\tilde{c}_3R+\tilde{c}_4\frac{R^2}{6}\right)\frac{dQ_2}{dt}-Q_2\left(\frac{\tilde{c}_3}{2}+\tilde{c}_4R+\tilde{c}_5\frac{R^2}{6}\right)\frac{dH}{dt}+\frac{1}{2}F_2\right], \tag{21}$$

where

$$F_1=Q_1^2\left(c_2^2-2c_2c_3R+(3c_3^2-4c_2c_4)\frac{R^2}{3}\right),$$

$$F_2=Q_2^2\left(\tilde{c}_2^2-2\tilde{c}_2\tilde{c}_3R+(3\tilde{c}_3^2-4\tilde{c}_2\tilde{c}_4)\frac{R^2}{3}\right),$$

and $\mu=\rho_2/\rho_1$ denotes the density ratio. Here, the expressions for c_n are

$$c_1=\frac{k}{e^{kH}-1},\quad c_2=-\frac{k^2e^{kH}}{(e^{kH}-1)^2},\quad c_3=\frac{k^3e^{kH}(e^{kH}+1)}{(e^{kH}-1)^3},$$

$$c_4=-\frac{k^4e^{kH}(e^{2kH}+4e^{kH}+1)}{(e^{kH}-1)^4},$$

$$c_5=\frac{k^5e^{kH}(e^{3kH}+11e^{2kH}+11e^{kH}+1)}{(e^{kH}-1)^5},$$

and $\tilde{c}_n(H)=c_n(-H)$. Note that c_n, $1\leq i\leq 5$, are identical to Zufiria's [7], setting $k=2$ $(L=\pi)$. The ordinary differential

equations (18)–(21) determine the dynamics of a single bubble of arbitrary density ratio.

We examine the range of validity of the modeling for the physical flow system. Differentiating the potentials (3) and (4), it gives

$$\frac{dW_1}{d\hat{z}} = Q_1 \frac{k}{e^{k(\hat{z}+H)}-1} - U, \tag{22}$$

$$\frac{dW_2}{d\hat{z}} = Q_2 \frac{k}{e^{k(\hat{z}-H)}-1} + K - U. \tag{23}$$

We see from Eq. (22) that, the fluid velocity decays exponentially from the interface to the heavy fluid, in laboratory frame. From Eqs. (23) and (18), it is easy to check that the velocity in the light fluid converges to $e^{-kH}(K-U)$ as $\hat{x}\to -\infty$. The model thus does not satisfy the zero flux condition at $\hat{x}\to-\infty$. We also find that the whole velocity field in the light fluid converges asymptotically to the bubble velocity, from the fact that $Q_2\to 0$ and $K\to U$ at a late time (see Sec. III). This behavior of the flow behind the bubble agrees, in near field, with the observation from numerical results in Ref. [8]: The vertical velocity in the light fluid flattens out near the bubble tip and the horizontal velocity goes to zero. Therefore, the present model gives an appropriate description to the flow near the bubble, and is not valid for the far field behind the bubble. The model assumes that the far field in the right fluid has little influence on the motion of the bubble front. This assumption will be validated at Sec. III by comparisons with numerical results.

III. SINGLE BUBBLE SOLUTIONS

In this section, we present the linear solution, the asymptotic solution, and the finite time solution of a single bubble from Zufiria's model, and compare with the results of other models and numerical simulations.

A. Linear solution

We first derive the linear solution of the Zufiria model. We show that, at small amplitude or linear stage, the Zufiria model agrees with the result of the linear stability analysis [2,3]. Note that the linear stability analysis, assuming that the small disturbance to the interface is proportional to $\exp(iky+\sigma t)$, gives $\sigma^2=Agk$, where $A=(\rho_1-\rho_2)/(\rho_1+\rho_2)$ is the Atwood number.

Assuming that the dimensionless curvature $(kR)^{-1}$ and dimensionless velocity $\sqrt{k^3/g}Q$ are small, Eqs. (19) and (20) are approximated as

$$\frac{d\xi}{dt} = c_3 Q_1 = \tilde{c}_3 Q_2, \tag{24}$$

$$c_2\frac{dQ_1}{dt} + c_3 Q_1 \frac{dH}{dt} + g\xi = \mu\left(\tilde{c}_2\frac{dQ_2}{dt} - \tilde{c}_3 Q_2\frac{dH}{dt} + g\xi\right). \tag{25}$$

Here, $\xi=1/R$ represents the bubble curvature.

Equation (25) can be written as

$$\frac{d}{dt}(c_2Q_1) + g\xi = \mu\left(\frac{d}{dt}(\tilde{c}_2Q_2) + g\xi\right). \tag{26}$$

One can check that $\tilde{c}_2Q_2=-c_2Q_1$, from Eq. (24) and the expressions of c_n and $\tilde{c}_n$. Then, defining $\Gamma=c_2Q_1$, Eq. (26) reduces to

$$\frac{d\Gamma}{dt} = -Ag\xi. \tag{27}$$

Differentiating this equation and using Eq. (24), we have

$$\frac{d^2\Gamma}{dt^2} = -\frac{c_3}{c_2}Ag\Gamma = \frac{1+\delta}{1-\delta}Agk\Gamma, \tag{28}$$

recalling $\delta=e^{-kH}$. From Eq. (10), the assumption $\xi/k\ll 1$ follows $\delta\ll 1/2$. Then, Eq. (28) behaves approximately as

$$\frac{d^2\Gamma}{dt^2} = Agk\Gamma, \tag{29}$$

which gives $\Gamma\sim\sinh(\sigma t)$ with $\sigma=\sqrt{Agk}$. From the definition of Γ and Eq. (18), the velocity has the solution $U\sim\sinh(\sigma t)$, and therefore $X\sim\cosh(\sigma t)$. The amplitude of the interface approximately has the exponential growth with the rate σ, which agrees with the linear stability analysis.

B. Asymptotic solution

The system of ordinary differential equations (18)–(21) has a critical point which corresponds to a steady rising bubble. The critical point (or, asymptotic solution) can be easily obtained by setting all time derivatives of variables to zero in Eqs. (19)–(21). Then, the asymptotic solution for a bubble in the RT instability is

$$R\to\frac{\sqrt{3}}{k},\quad H\to\frac{1}{k}\ln(2+\sqrt{3}),\quad Q_1\to\frac{2}{3^{1/4}}\sqrt{\frac{2Ag}{(1+A)k^3}},$$

$$U\to\frac{\sqrt{6+4\sqrt{3}}}{2+\sqrt{3}}\sqrt{\frac{2Ag}{3(1+A)k}},\quad Q_2\to 0,\quad K\to U. \tag{30}$$

We see that the bubble converges to the constant limit, forgetting the initial condition. The asymptotic solution was also reported in Sohn [10] and the derivation is found there. From Eqs. (11) and (30), we find the asymptotic bubble width by $\lambda=0.73L$, which is slightly larger than the diameter of the bubble curvature $2R\to 0.55L$.

The asymptotic bubble velocity in Eq. (30) has a similar functional form with the solution of the Layzer model, obtained by Goncharov [8], except the factor $\sqrt{6+4\sqrt{3}}/(2+\sqrt{3})=0.963$. However, the asymptotic bubble curvatures from two models have quantitatively a large difference. The solution of the Layzer model is $\xi_{\text{Layzer}}\to k/3$, while in the Zufiria model, $\xi_{\text{Zufiria}}\to k/\sqrt{3}$ from Eq. (30). This discrepancy may be due to the fact that the bubble curvature is a much more sensitive variable than the bubble velocity and the

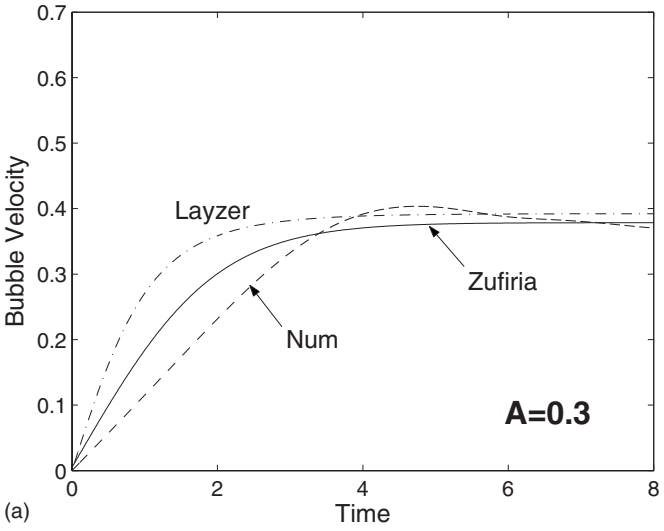

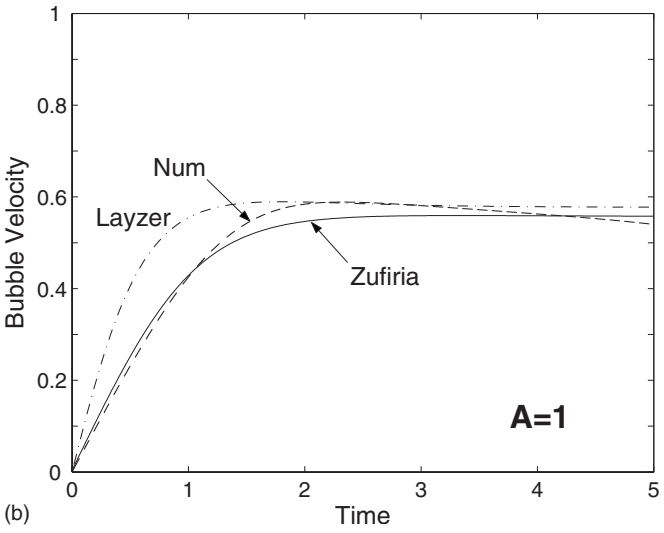

FIG. 2. Bubble velocity for (a) $A=0.3$ and (b) $A=1$.

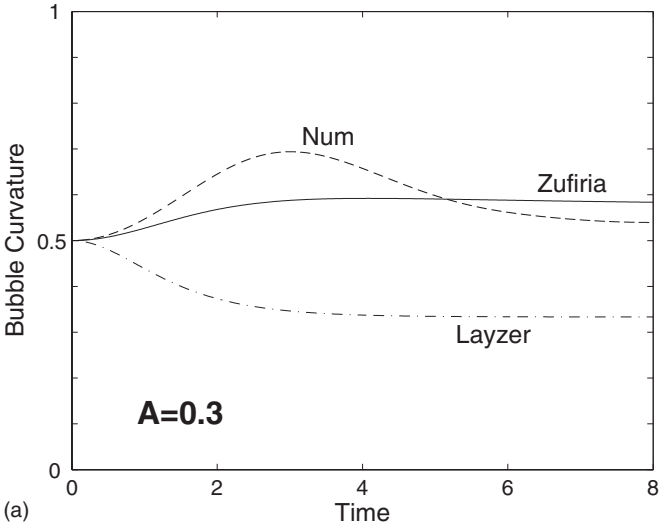

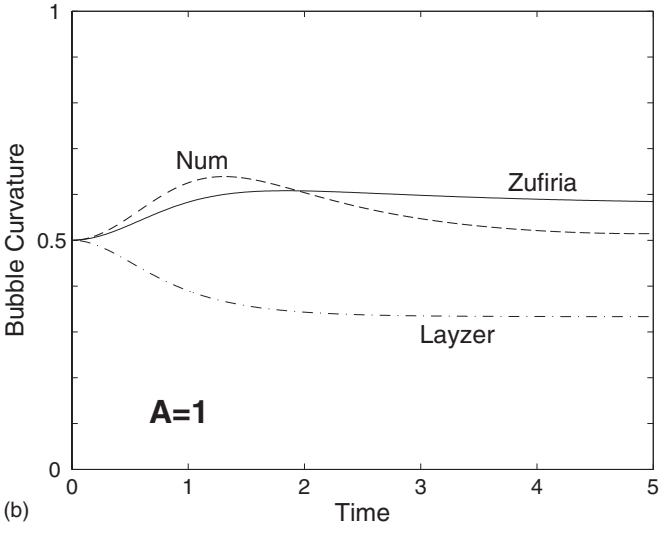

FIG. 3. Bubble curvature for (a) $A=0.3$ and (b) $A=1$.

Layzer model takes only the first harmonic in the velocity potential. Adding higher mode harmonics to the potential in Layzer's model, the difference of the asymptotic curvatures from two models may be reduced.

C. Finite time solution

We now investigate the agreement of the models by comparing the finite time solutions of the models with numerical results. The solutions for finite times can be obtained by solving Eqs. (18)–(21) numerically. Differentiating Eqs. (18) and (19), dQ_2/dt and dK/dt in Eqs. (20) and (21) can be expressed in terms of dQ_1/dt, dH/dt, and other variables. Then, Eqs. (20) and (21) become ordinary differential equations of dQ_1/dt and dH/dt, so that they can be integrated. For numerical integrations, we employ the standard fourth order Runge-Kutta method. The initial conditions are determined from a given initial amplitude and velocity. $R(t=0)$ can be set from the initial amplitude, assuming a sinusoidal shape, and $H(t=0)$ is given by Eq. (10). Then, $Q_1(t=0)$ is set by Eq. (18) and the initial velocity, $Q_2(t=0)$ by Eq. (19), and $K(t=0)$ by Eq. (18).

All results in this section are plotted in dimensionless units. The dimensionless time, velocity, and curvature are given by $t\sqrt{kg}$, $U\sqrt{k/g}$, and ξ/k, respectively.

In Fig. 2, we compare the solutions for the bubble velocity from the Zufiria model with numerical results taken from Ref. [26], and the solutions of the Layzer model [8]. The numerical simulations in Ref. [26] are performed by the vortex method and the solutions of the Layzer model are obtained by integrating Eqs. (7) and (8) in Ref. [8]. The left and right plots in Fig. 2 correspond to the cases of $A=0.3$ (density ratio 1.86:1) and $A=1$ (fluid and vacuum), respectively. The physical parameters are $g=1$ cm/s^2 and $k=1$ cm^{-1}, and the initial amplitude and velocity are 0.5 cm and 0, respectively. Figure 2 shows that, for both cases, the solutions of the Zufiria model for the bubble velocity agrees better with the numerical results than with the Layzer model over all time ranges. The predictions for the asymptotic velocity are in excellent agreement for both models, but the Zufiria model fits slightly better with the numerical results. We men-

tioned that the analytic solutions for the asymptotic velocity from both models differ only in the factor 0.963. Therefore, 0.963 in the asymptotic solution of the Zufiria model plays a correction factor from the Layzer model.

Figure 3 plots the solutions for the bubble curvature from two models and the numerical results, for the same cases in Fig. 2. Figure 3 shows that the Zufiria model provides qualitatively good predictions for the bubble curvature, while the solutions of the Layzer model deviate from the numerical results. Figure 3 raises a question of the independence of density ratios for the asymptotic bubble curvature. Both theoretical models predict the constant asymptotic bubble curvature, independent to the density ratio, while the numerical solutions converge to slightly different limits between 0.5 and 0.55. Note that the numerical method in Ref. [26] has a regularization parameter for the finite density ratio cases, which leads to the smoothing effect to the solution. In fact, few numerical results have been reported for the bubble curvature of finite density ratio, although numerical simulations for the single-mode RT instability have been performed by many authors using various numerical methods [27–31]. Therefore, the independence of density ratios for the asymptotic bubble curvature is not concluded at the current stage and this will be the subject of future researches.

IV. MULTIPLE BUBBLE MODEL

The single bubble model is here extended to multiple bubbles of arbitrary density ratio. We follow the similar approach as the infinite density ratio case in Zufiria [7]. The channel of width L contains N distinct bubbles and the positions of the bubble tips are $Z_i=X_i+\mathrm{i}Y_i$, $i=1,2,\ldots,N$. We assume that the horizontal positions of bubbles Y_i are constants, neglecting lateral effects. The potentials for multiple bubbles can be constructed as the sum of the potential for each bubble. Then, the potentials for the bubbles are

$$W_1^i(\hat{z}) = \sum_{j=1}^{N} Q_1^j[\ln(1-e^{k/2(Z_j-H_j-Z_i-\hat{z})}) + \ln(1-e^{k/2(Z_j^*-H_j-Z_i-\hat{z})})] - U_i\hat{z}, \tag{31}$$

$$W_2^i(\hat{z}) = \sum_{j=1}^{N} Q_2^j[\ln(1-e^{k/2(Z_j+H_j-Z_i-\hat{z})}) + \ln(1-e^{k/2(Z_j^*+H_j-Z_i-\hat{z})})] + (K_i-U_i)\hat{z}, \tag{32}$$

for $i=1,\ldots,N$, where the * denotes the complex conjugate.

In Eqs. (31) and (32), the method of images is applied for the modeling of the wall. That is to say, for each potential, the image potential is placed at the conjugate point. One can imagine that the symmetric bubbles lie in the region $-L \leqslant Y \leqslant 0$. Then, the flow is periodic with the period $2L$ and the line $Y=0$ becomes a streamline by the symmetry, which is regarded as a wall.

The potentials (31) and (32), after the expansions with respect to $\hat{z}$, have the form

$$W_1^i = \sum_{j=1}^{N}\left(Q_1^j\sum_{n=0}^{\infty}\frac{c_n^{ij}}{n!}\hat{z}^n\right) - U_i\hat{z}, \tag{33}$$

$$W_2^i = \sum_{j=1}^{N}\left(Q_2^i\sum_{n=0}^{\infty}\frac{\tilde{c}_n^{ij}}{n!}\hat{z}^n\right) + (K_i-U_i)\hat{z}. \tag{34}$$

Here, the coefficients c_n^{ij} and $\tilde{c}_n^{ij}$ have complex values, and are denoted as $c_n^{ij}=a_n^{ij}+\mathrm{i}b_n^{ij}$ and $\tilde{c}_n^{ij}=\tilde{a}_n^{ij}+\mathrm{i}\tilde{b}_n^{ij}$. The expressions of c_n^{ij} and $\tilde{c}_n^{ij}$ are given in the Appendix. Note that the relations $c_{n+1}^{ij}=dc_n^{ij}(H_j)/dH_j$ and $\tilde{c}_{n+1}^{ij}=d\tilde{c}_n^{ij}(H_j)/dH_j$, $n\geqslant 0$, hold, similarly as the single bubble case.

Satisfying the boundary equations (12) and (13) with the potentials (33) and (34), one can derive a $4N$ system of ordinary differential equations. These equations are given by

$$\frac{dX_i}{dt} = U_i = \sum_j a_1 Q_1^j = \sum_j \tilde{a}_1 Q_2^j + K_i, \tag{35}$$

$$\frac{dR_i}{dt} = -\sum_j Q_1^j(3a_2+a_3R_i)R_i = -\sum_j Q_2^j(3\tilde{a}_2+\tilde{a}_3R_i)R_i, \tag{36}$$

$$\sum_j (a_1+a_2R_i)\frac{dQ_1^j}{dt} + \sum_j Q_1^j(a_2+a_3R_i)\frac{dH_j}{dt} - [(p_2^i)^2+(q_2^i)^2]R_i + g = \mu\left[\sum_j (\tilde{a}_1+\tilde{a}_2R_i)\frac{dQ_2^j}{dt} + \frac{dK_i}{dt} - \sum_j Q_2^j(\tilde{a}_2+\tilde{a}_3R_i)\frac{dH_j}{dt} - [(\tilde{p}_2^i)^2+(\tilde{q}_2^i)^2]R_i + g\right], \tag{37}$$

$$\sum_j\left(\frac{a_2}{2}+a_3R_i+a_4\frac{(R_i)^2}{6}\right)\frac{dQ_1^j}{dt} + \sum_j Q_1^j\left(\frac{a_3}{2}+a_4R_i+a_5\frac{(R_i)^2}{6}\right)\frac{dH_j}{dt} + \frac{F_1^i}{2} = \mu\left[\sum_j\left(\frac{\tilde{a}_2}{2}+\tilde{a}_3R_i+\tilde{a}_4\frac{(R_i)^2}{6}\right)\frac{dQ_2^j}{dt} - \sum_j Q_2^j\left(\frac{\tilde{a}_3}{2}+\tilde{a}_4R_i+\tilde{a}_5\frac{(R_i)^2}{6}\right)\frac{dH_j}{dt} + \frac{F_2^i}{2}\right], \tag{38}$$

where

$$F_1^i = (p_2^i)^2+(q_2^i)^2-2(p_2^ip_3^i+q_2^iq_3^i)R_i + \left((p_3^i)^2+(q_3^i)^2-\frac{4}{3}(p_2^ip_4^i+q_2^iq_4^i)\right)R_i^2, \tag{39}$$

$$F_2^i = F_1^i(p_n^i\rightarrow\tilde{p}_n^i, q_n^i\rightarrow\tilde{q}_n^i), \tag{40}$$

for $i=1,\ldots,N$. Here, p_n^i, q_n^i and $\tilde{p}_n^i, \tilde{q}_n^i$ are defined by

$$p_n^i = \sum_j Q_1^i a_n^{ij}, \quad q_n^i = \sum_j Q_1^i b_n^{ij},$$

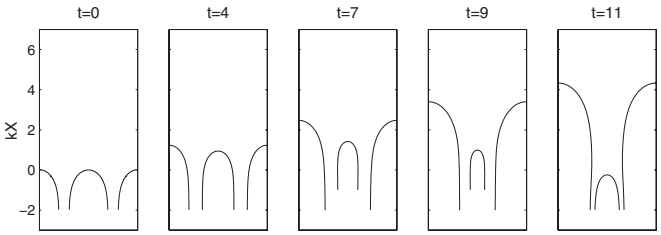

FIG. 4. Evolution of three bubbles. The Atwood number is $A=0.5$.

$$\tilde{p}_n^i = \sum_j Q_2^i \tilde{a}_n^{ij}, \quad \tilde{q}_n^i = \sum_j Q_2^i \tilde{b}_n^{ij}.$$

In Eqs. (35)–(38), the superscripts of a_n^{ij}, b_n^{ij}, $\tilde{a}_n^{ij}$, and $\tilde{b}_n^{ij}$ are suppressed for short notations. The system of differential equations (35)–(38) determine the motions of the N bubbles.

V. MULTIPLE BUBBLE SOLUTIONS

We apply the model to the multiple bubbles to simulate the bubble interaction process. We assume that N identical bubbles in the channel of width L are equally spaced along the horizontal direction, i.e.,

$$Y_i = \frac{(i-1)L}{N-1}, \quad i = 1, \ldots, N.$$

If all bubbles have the same initial conditions, they grow equally and converge to the asymptotic solution of a single bubble of the channel width L/N. To give the interaction between bubbles, we give perturbations to the longitudinal positions of bubbles. The initial velocity and radius of bubbles are set as

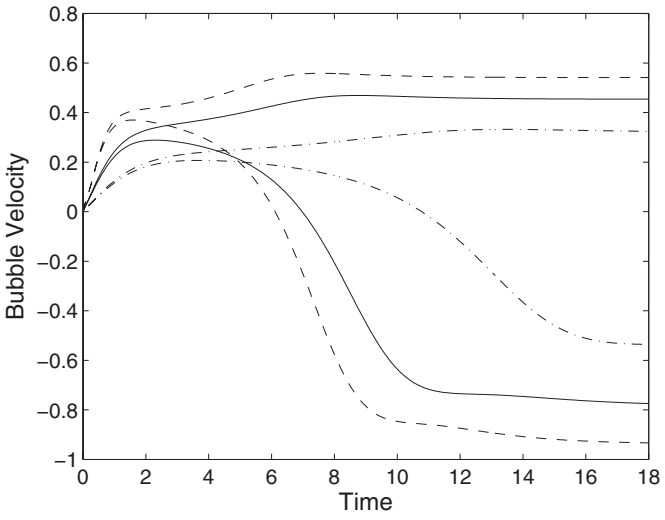

FIG. 5. Bubble velocity for $N=3$ for selected Atwood numbers. The dashed curves correspond to $A=0.9$, the solid curves to $A=0.5$, and the dash-dotted curves to $A=0.2$.

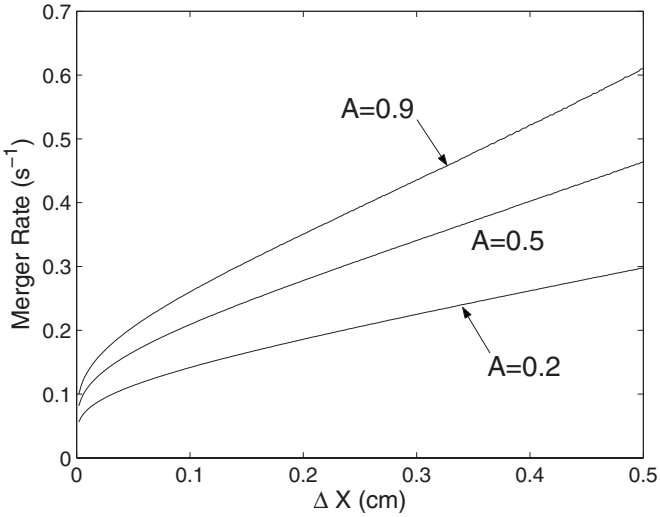

FIG. 6. Merger rate versus $\Delta X(t=0)$ for selected Atwood numbers.

$$U_i = 0, \quad R_i = \frac{R^0}{N-1}, \quad i = 1, \ldots, N, \tag{41}$$

where R^0 is a given constant. For all results in this section, R^0 is set to 2 cm. Note that the perturbation on the radii of bubbles has similar effects as that on the longitudinal positions.

Equations (35)–(38) are first applied to three bubble interactions as a simple case. Figure 4 displays the evolution of three bubbles for the Atwood number $A=0.5$. The units in Fig. 4 (and Figs. 5 and 8) are dimensionless, as defined in Sec. III. The physical parameters are set to $g=1$ cm/s^2 and $k=1$ cm^{-1}. The initial bubble heights are $X_1=X_3=0.1$ cm and $X_2=0$. In Fig. 4, we find that the three bubbles advance and compete for a while. The higher bubble expands and grows faster than the lower one, while the lower bubble shrinks and grows slower, and then is washed downstream, after reaching

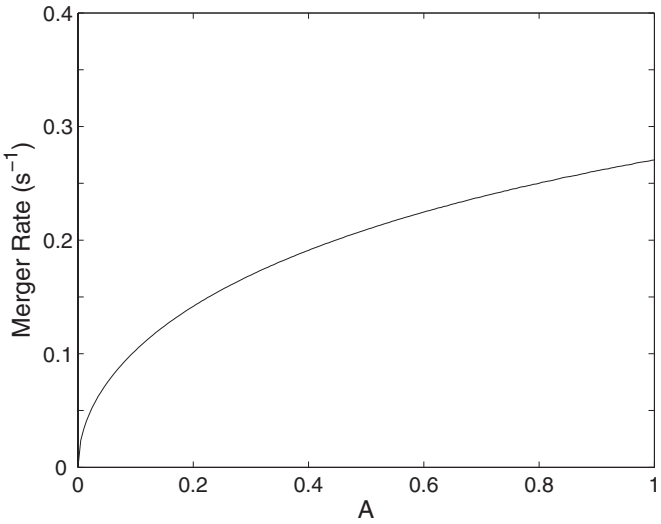

FIG. 7. Merger rate versus the Atwood number. ΔX is set to 0.1 cm.

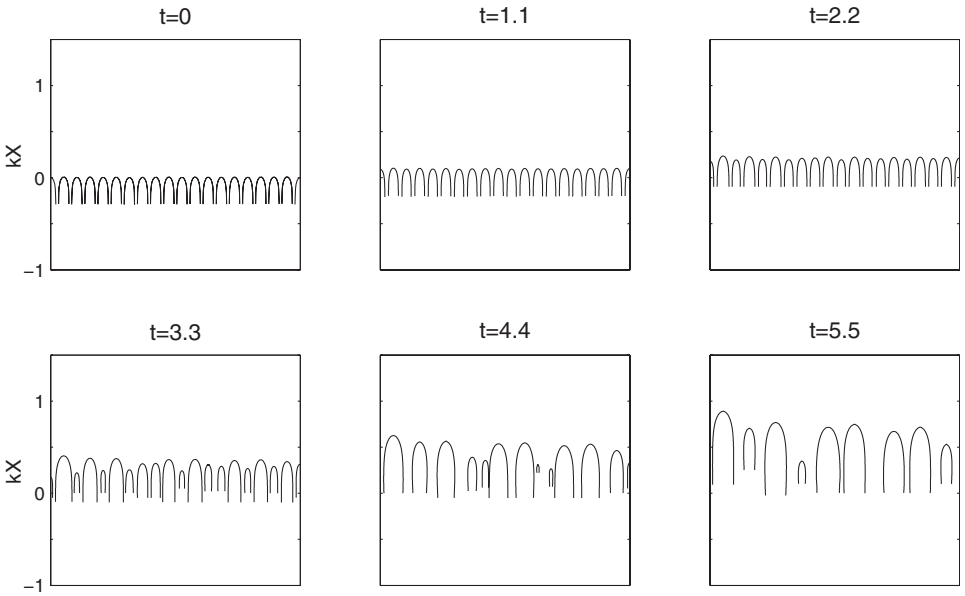

FIG. 8. Evolution of multiple bubbles with $N=20$. The Atwood number is $A=0.5$.

a maximum around $t=7$. In fact, the higher bubble finally attains the asymptotic velocity and radius of a single bubble of the channel width. Therefore, the front of the channel is eventually filled with the higher bubble. In Fig. 4, the smaller bubble tends to recover its size when it is in the far downstream. This behavior is due to the incorrect description of the model for the flow in the far field behind the bubble [7]. In reality, the spikes are formed at the back of the bubble and the smaller bubble merges into the spike region. We see from Figs. 4 (and 5) that the dynamics in the far field give little influence to the motion of the front bubble.

Figure 5 shows the bubble velocity of $N=3$ for selected Atwood numbers. The dashed curves correspond to $A=0.9$, the solid curves to $A=0.5$, and the dash-dotted curves to $A=0.2$. The initial conditions are the same as Fig. 4. In Fig. 5, the solutions of the first and third bubble are overlapped, since two bubbles are the same except the horizontal position. We observe that the bubble velocities are nearly the same at early times and saturate with around the asymptotic velocity of a single bubble of the half channel width. The competition begins as the velocities saturate, and then the higher bubble accelerates and the lower bubble decelerates. Finally, the higher bubble converges to the asymptotic solution of a single bubble of the whole channel width. We also find that, for a smaller Atwood number, it takes longer competition time and the bubble front has a smaller growth rate.

To quantify the competition time, we consider the merger rate of three bubbles. From the criterion in Refs. [17–19], the merger time is defined by $\tau=t_b-t_a$ and the merger rate by $1/\tau$, where t_a is the time when the velocity of a smaller bubble has a maximum and t_b the time when it becomes zero. Figure 6 plots the merger rates with respect to the difference of initial bubble heights $\Delta X=X_1-X_2$ for selected Atwood numbers. For all cases, the merger rates are increasing functions for ΔX, so that the bubbles merge faster for larger initial perturbations. For fixed ΔX, the merger rate is reduced as the density ratio decreases, as indicated in Fig. 5. Note that the merger rate is zero at $\Delta X=0$. Figure 7 is the merger rate with respect to the Atwood number. The initial longitudinal perturbations are set to $\Delta X=0.1$ cm. We see that the merger rate is an increasing function for the Atwood number and it quickly reduces for small Atwood numbers.

Figure 8 illustrates the evolution of 20 bubbles for $A=0.5$. Initially, the longitudinal positions of bubbles X_i are randomly perturbed in the interval $[0,0.01]$ cm. Figure 8 clearly shows the interaction process of bubbles. At early times, the bubbles move forward and compete with each other, and then the higher bubbles grow faster and expand, and the number of bubbles at the front decreases. Only nine bubbles survived at $t=5.5$ in Fig. 8. Figure 9 is the bubble positions versus Agt^2 for Fig. 8. We see that the bubble front grows linearly in t^2. We have checked that the results for different Atwood numbers have similar behaviors as Figs. 8 and 9, and the difference is a faster (slower) evolution for larger (lower) density ratio.

We have run simulations for $N=20$ for several Atwood numbers, to estimate the growth coefficient α of the scaling law (1). Figure 10 shows the result of the model for the coefficient α with respect to the Atwood number. The value

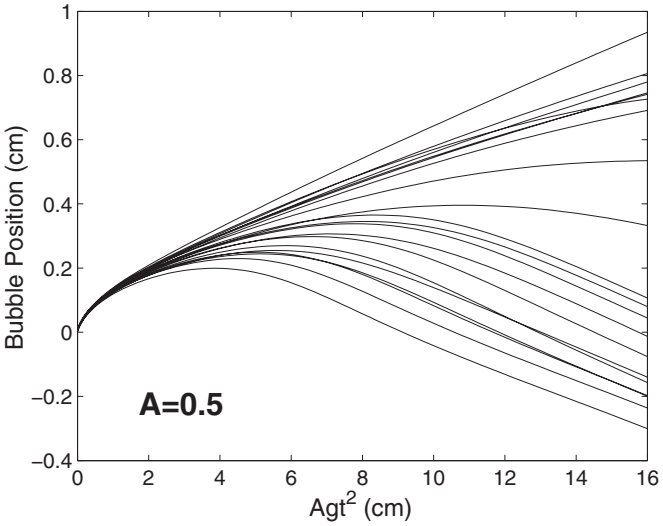

FIG. 9. Bubble position versus Agt^2 for Fig. 8.

of α in Fig. 10 ranges from 0.041 to 0.072. Previous results for α, in two dimensions, are $\alpha \sim 0.058-0.065$ from the experiments by Read [14] and $\alpha \sim 0.04-0.05$ from the numerical simulations by Youngs [15,16]. The results using front tracking methods by Glimm *et al.* [32] found $\alpha \sim 0.06$ on average, and simulations using lattice Boltzmann methods by Clark [33] gave $\alpha \sim 0.05$ on average. Our result gives the average value of $\alpha \sim 0.057$, and therefore agrees well with the previous results. Note that the growth of the mixing zone may be varied by physical factors such as initial conditions, dimensions, surface tension, diffusion, and viscosity. In Fig. 10, we also observe an interesting behavior that α slightly depends on the density ratio and is smaller for a larger Atwood number. This result is in accordance with LEM (linear electric motor) experiments in three dimensions by Dimonte and Schneider [34], which gave $\alpha \sim 0.053 \pm 0.06$ for $A < 0.5$ and $\alpha \sim 0.049 \pm 0.003$ for $A > 0.8$. The recent experiment by Banerjee and Andrews [35] measures $\alpha \sim 0.065-0.07$ for small Atwood numbers, $0.035 < A < 0.1$. For the validation of the downward behavior of α, more comprehensive experiments and numerical simulations are called for.

There is a difference between our result and Zufiria [7] for the prediction of α. The growth coefficient for $A=1$ in Fig. 10 is $\alpha \sim 0.041-0.045$, while Zufiria reported $\alpha \sim 0.049-0.055$, for the same initial random perturbations X_i in the interval $[0, 0.01]$ cm with the number of bubbles $N=20$. This is due to different settings of the the wave number (or the channel width) and the initial velocity. The channel width considered here is twice larger than that in Zufiria. Moreover, the initial velocity is set to 0 in our simulations, while in Zufiria, the asymptotic velocity of a single bubble is used for the initial velocity, in order to reduce the transient time for bubble interactions. If the channel width is reduced by half, or the asymptotic velocity is used for the initial condition in our simulations, the value of α increases by around 0.005. When both the channel width and the initial velocity are set to the same as Zufiria, we recover the result $\alpha \sim 0.049-0.055$.

It has been known that the ratio of the bubble width to the bubble height has a self-similar behavior [17,23,34,36–39]. To examine this, we use the diameter of the bubble curvature instead of the bubble width, because it is easier to evaluate in the present model and is comparable to the bubble width, as shown for the single bubble case. Figure 11 plots the ratio $\beta = 2\bar{R}/h$ with respect to Agt^2 for $A=0.5$ for various runs, where $\bar{R}$ is defined as the average radius of curvatures of bubbles with positive velocities. We find in Fig. 11 that, in the scale invariant regime, β has the minimum of 0.43 and the maximum of 0.67, and the average for each run ranges between 0.5 and 0.6. Therefore, the RT bubbles indeed grow self-similarly with the the aspect ratio β. Figure 12 is the averages of the similarity ratio β in the scale invariant regime with respect to the Atwood number. The values of β are in the range of 0.48 and 0.61, and slightly increase with the Atwood number. This result is consistent with the LEM experiments [34], and theoretical predictions by Mikaelian [36] and Dimonte [39]. The values for β of these results are quantitatively in similar range, but the dependence on the Atwood number differs. The LEM experiments obtain $\beta \sim 0.3(1+A)$,

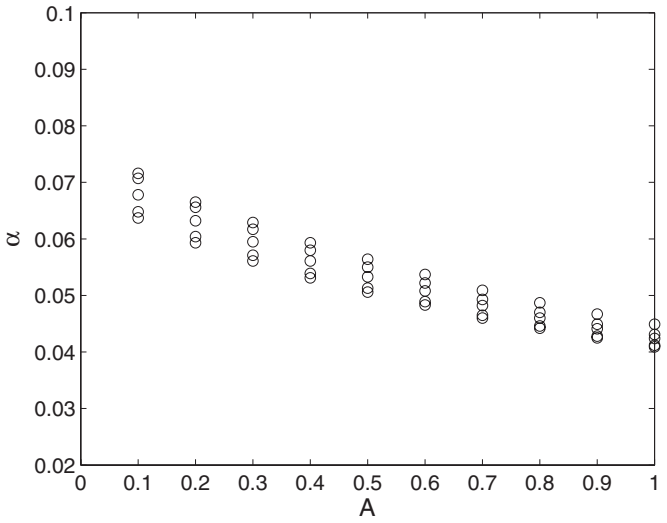

FIG. 10. Growth coefficients α versus the Atwood number.

which has a larger slope with A than the present model. Comparing Figs. 10 and 12, we find that the parameter β is less sensitive to the Atwood number than α.

A variety of high-resolution three-dimensional numerical simulations have recently been employed for the turbulent RT instability [40–42], and reported that the growth constant α depends on initial conditions. Dimonte [39] proposed a mode-competition model to quantify the effect of initial conditions. We mentioned the dependence of α on the wave number (or the channel width) in the present model, and this fact already reflects the dependence of the bubble evolutions on the initial conditions. For further investigations on the initial conditions, we run simulations for various initial random perturbations. Figure 13 shows variations of the growth constant α with respect to initial perturbation amplitudes for the Atwood numbers $A=0.3$ and $A=1$. The number of bubbles are $N=20$ and the wave number is $k=1$ cm^{-1}. We observe a logarithmic increase of α with respect to the initial perturbation amplitude for both cases. These results on the

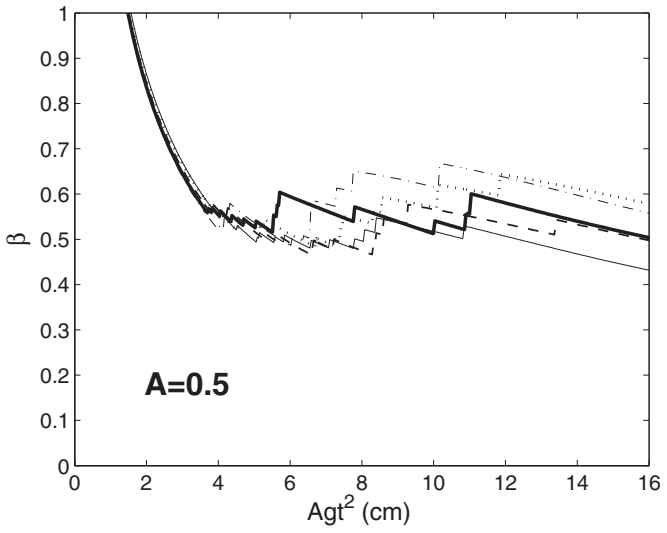

FIG. 11. Self-similarity ratio $\beta = 2\bar{R}/h$ versus Agt^2 for $A=0.5$.

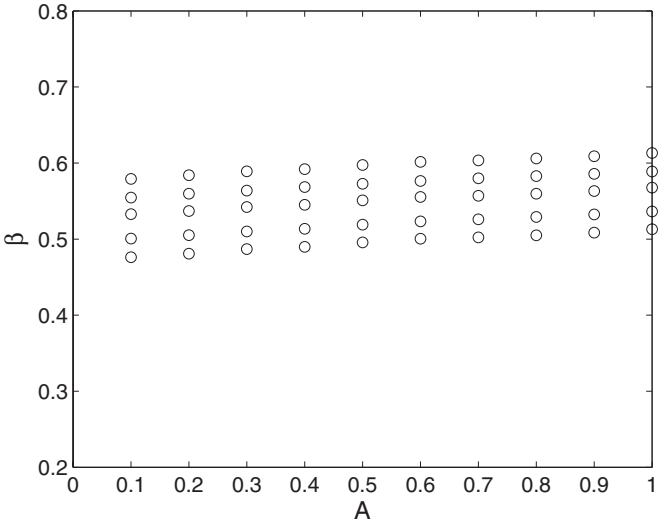

FIG. 12. Self-similarity ratio β versus the Atwood number. The values of β are averages in the scale invariant regime.

variation of α for the initial perturbation amplitude agree with the mode-competition model [39] and numerical simulations [42].

VI. DISCUSSION AND CONCLUSIONS

The potential flow model with moving source singularities has been extended to the unstable interface of finite density ratio. We have presented the solutions for a single bubble, at different stages, and investigated the dynamics of the multiple bubble interactions.

We have shown that the Zufiria-type model provides comprehensive descriptions for the evolution of bubbles. The Zufiria model gives the exponential growth rate at the linear stage, and the predictions for the bubble curvature, as well as the bubble velocity, from the model agrees better with the numerical results than the Layzer model. The quantitative differences between two models for the solutions come from the choice of potentials, and therefore the source-type potential is more appropriate for the description of the unstable interface than the potential of a sinusoidal form.

The comparison of the solution for a single bubble with the numerical results raised the issue of the independence of density ratios for the asymptotic curvature. The model gives the constant asymptotic curvature, while the numerical results slightly varies with the density ratio. To know this question, fine scale computations with zero viscosity and surface tension are needed. However, long-time simulations for the RT instability under those conditions are, in fact, very difficult and it might be necessary to develop more advanced numerical methods.

Several models for the extension of a single RT bubble to finite density ratio have been proposed, but a complete modeling is still not accomplished. The present model and the extension of Layzer's model [8] do not satisfy the zero velocity condition at negative infinity, allowing a mass flux. The model in Abarzhi *et al.* [12] satisfies the boundary conditions, but does not give good predictions for the bubble velocity and curvature for overall Atwood numbers. A theory

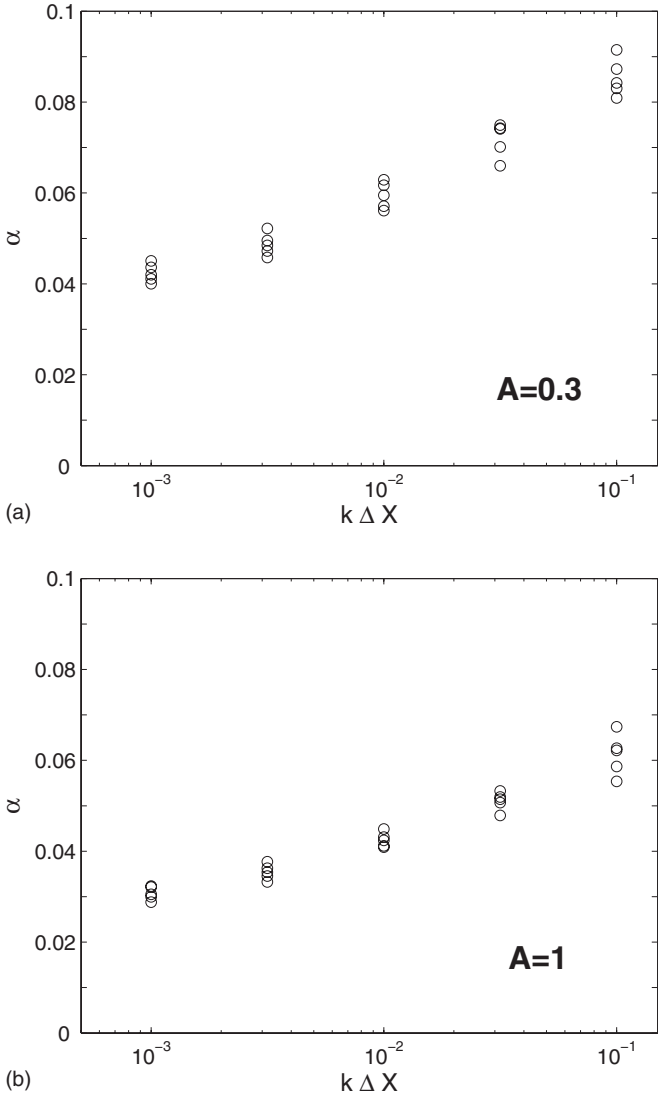

FIG. 13. Variation of α with respect to initial random perturbation amplitudes for (a) $A=0.3$ and (b) $A=1$.

which simultaneously satisfies the boundary conditions and gives correct solutions for a single RT bubble, has not been established yet, and is remained for development.

The Zufiria model has successfully demonstrated the bubble competition process in the system of finite density ratio. For the random perturbations of the RT instability, it is difficult to draw unified conclusions from numerical simulations, because numerical results have usually been reported only for limited values of the Atwood number, due to high computation costs, and the results depend on the numerical method and zoning. The potential flow model provides the simple equations for the motion of bubbles, so that it is capable to simulate the multiple bubble evolutions for a wide range of the Atwood number. The results of the model for the scaling law of the bubble front showed good agreements with the experimental and numerical results. The growth constant α and the aspect ratio β of the bubble size to the height have dependence on the density ratio. The model predicts that the similarity parameter β exhibits an opposite slope to α with respect to the Atwood number, and its dependence is weaker than α.

Theoretical models to estimate α differ by their description of self-similarity. The models proceed in two limiting ways, namely, by the nonlinear coupling of two or more bubbles to form a larger structure (merger) and by the growth and saturation of ambient modes (competition). The bubble merger models involve the nonlinear coupling of saturated modes ($h \sim 1/k$), and thus may produce a universal α [17,19,20,23]. The mode-competition model predicts variations of α on the Atwood number and the initial perturbations [39]. The results of the Zufiria model for the self-similarity parameters are consistent with the mode-competition model.

The present model gives an appropriate description for the flow near the interface and assumed that the far field behind the bubble has little influence on the motion of the bubble front. Although this assumption was validated by comparisons with the numerical results, the dynamics of bubbles might be influenced by secondary Kelvin-Helmholtz instabilities around spikes at late nonlinear stage, or turbulent stage, when vorticities are prominent and critically strong. Recently, Ramaprabhu *et al.* [43] studied the validity regime of potential flow models and the influences of vorticities on the bubble motion. It is observed that a single-mode RT bubble of low density difference exhibits a late-time reacceleration, due to the strong Kelvin-Helmholtz roll-up, while for large density ratio, the formation of the secondary instability is suppressed and the terminal bubble velocity remains constant. The Kelvin-Helmholtz instability may also affect the bubble competition process, and thus might produce higher values of α than the predictions from the Zufiria model, at fully turbulent stages for low density ratios.

The bubble evolutions in two dimensions (2D) have been presented by the Zufiria model, but the mixing by RT instability occurs in three dimensions (3D) in reality. There are several differences from the dimensionality on the bubble interaction dynamics. The asymptotic velocity of a single bubble increases in 3D by about a factor of 1.5 [8,9]. A 3D bubble has to overcome more of its neighbors, while a bubble in 2D competes with only two neighbors. These two factors have opposite effects on the growth rate and may explain the result in Youngs [44]: The kinetic energy is less dissipated in 2D than 3D, and therefore the 3D mixing zone grows more rapidly than 2D at early times and slows down when the turbulence develops. We also note that slightly larger values of α in 3D than 2D were reported in comparison studies [14,23,38,44,45], albeit some quantitative variations.

A similar type of the unstable interface as the RT instability is the Richtmyer-Mehksov instability [4,5,46], which is driven by a shock wave, and the mixing by this instability has also been studied intensively. The applications of the potential flow model to bubble interactions of the shock-induced instability will be the next step of the research.

ACKNOWLEDGMENTS

This work was supported by the Korea Research Foundation Grant funded by the Korean Government (MOEHRD) under Grant No. KRF-2006-312-C00055.

APPENDIX

The full expressions of the coefficients $c_n^{ij}=a_n^{ij}+ib_n^{ij}$ in Eq. (33), up to $n=5$, are given here.

$$a_1^{ij}=\frac{k\epsilon}{2}\sum_{m=1}^{2}\frac{r_m-\epsilon}{d_m},\quad b_1^{ij}=\frac{k\epsilon}{2}\sum_{m=1}^{2}\frac{s_m}{d_m},$$

$$a_2^{ij}=-\frac{k^2\epsilon}{4}\sum_{m=1}^{2}\frac{-2\epsilon+(1+\epsilon^2)r_m}{d_m^2},\quad b_2^{ij}=\frac{k^2\epsilon(\epsilon^2-1)}{4}\sum_{m=1}^{2}\frac{s_m}{d_m^2},$$

$$a_3^{ij}=\frac{k^3\epsilon(1-\epsilon^2)}{8}\sum_{m=1}^{2}\frac{(1+\epsilon^2)r_m+\epsilon(-4+2r_m^2)}{d_m^3},$$

$$b_3^{ij}=\frac{k^3\epsilon}{8}\sum_{m=1}^{2}\frac{[1-6\epsilon^2+\epsilon^4+2(\epsilon+\epsilon^3)r_m]s_m}{d_m^3},$$

$$a_4^{ij}=-\frac{k^4\epsilon}{16}\sum_{m=1}^{2}\frac{\eta_m}{d_m^4},$$

$$b_4^{ij}=\frac{k^4\epsilon(\epsilon^2-1)}{16}\times\sum_{m=1}^{2}\frac{[1+\epsilon^4+8\epsilon(1+\epsilon^2)r_m+\epsilon^2(-22+4r_m^2)]s_m}{d_m^4},$$

$$a_5^{ij}=\frac{k^5\epsilon(1-\epsilon^2)}{32}\sum_{m=1}^{2}\frac{\zeta_m}{d_m^5},$$

where

$$d_m=1+\epsilon^2-2\epsilon r_m,$$

$$\eta_m=r_m+\epsilon^6 r_m-16\epsilon^3(-2+r_m^2)+8\epsilon(1+\epsilon^4)(-1+r_m^2)+\epsilon^2 r_m(1+\epsilon^2)(-13+4r_m^2),$$

$$\zeta_m=r_m+\epsilon^6 r_m+11\epsilon^2(1+\epsilon^2)r_m(-7+4r_m^2)+2\epsilon(1+\epsilon^4)(-8+11r_m^2)+4\epsilon^3(40-29r_m^2+2r_m^4),$$

for $m=1$, 2, and

$$\epsilon=e^{k/2(X_j-X_i-H_j)},$$

$$r_1=\cos\frac{k(Y_j-Y_i)}{2},\quad s_1=\sin\frac{k(Y_j-Y_i)}{2},$$

$$r_2=\cos\frac{k(Y_j+Y_i)}{2},\quad s_2=-\sin\frac{k(Y_j+Y_i)}{2}.$$

The expressions of $\tilde{c}_n^{ij}$ in Eq. (34) are followed by the relation $\tilde{c}_n^{ij}(H_j)=c_n^{ij}(-H_j)$.

[1] Lord Rayleigh, *Scientific Papers Vol. II* (Cambridge University Press, Cambridge, England, 1900), p. 200.
[2] G. I. Taylor, Proc. R. Soc. London, Ser. A **201**, 192 (1950).
[3] G. Birkhoff, *Proc. Symp. Appl. Math. Vol. XIII* (American Mathematical Society, Providence, 1962), p. 55.
[4] D. Sharp, Physica D **12**, 3 (1984).
[5] N. J. Zabusky, Annu. Rev. Fluid Mech. **31**, 495 (1999).
[6] D. Layzer, Astrophys. J. **122**, 1 (1955).
[7] J. Zufiria, Phys. Fluids **31**, 440 (1988).
[8] V. N. Goncharov, Phys. Rev. Lett. **88**, 134502 (2002).
[9] S.-I. Sohn, Phys. Rev. E **67**, 026301 (2003).
[10] S.-I. Sohn, Phys. Rev. E **70**, 045301(R) (2004).
[11] K. O. Mikaelian, Phys. Rev. E **67**, 026319 (2003).
[12] S. I. Abarzhi, J. Glimm, and A.-D. Lin, Phys. Fluids **15**, 2190 (2003).
[13] P. Ramaprabhu and G. Dimonte, Phys. Rev. E **71**, 036314 (2005).
[14] K. I. Read, Physica D **12**, 45 (1984).
[15] D. L. Youngs, Physica D **12**, 32 (1984).
[16] D. L. Youngs, Physica D **37**, 270 (1989).
[17] J. Glimm and D. H. Sharp, Phys. Rev. Lett. **64**, 2137 (1990).
[18] Q. Zhang, Phys. Lett. A **151**, 18 (1990).
[19] U. Alon, J. Hecht, D. Mukamel, and D. Shvarts, Phys. Rev. Lett. **72**, 2867 (1994).
[20] U. Alon, J. Hecht, D. Ofer, and D. Shvarts, Phys. Rev. Lett. **74**, 534 (1995).
[21] G. Dimonte, Phys. Plasmas **7**, 2255 (2000).
[22] B. Cheng, J. Glimm, and D. H. Sharp, Phys. Lett. A **268**, 366 (2000).
[23] B. Cheng, J. Glimm, and D. H. Sharp, Chaos **12**, 267 (2002).
[24] Y. Zhou, G. B. Zimmerman, and E. W. Burke, Phys. Rev. E **65**, 056303 (2002).
[25] L. M. Milne-Thompson, *Theoretical Hydrodynamics* (Dover, New York, 1968).
[26] S.-I. Sohn, Phys. Rev. E **69**, 036703 (2004).
[27] G. R. Baker, D. I. Meiron, and S. A. Orszag, Phys. Fluids **23**, 1485 (1980).
[28] G. Tryggvason, J. Comput. Phys. **75**, 253 (1988).
[29] W. Mulder, S. Osher, and J. A. Sethian, J. Comput. Phys. **100**, 209 (1992).
[30] X. He, S. Chen, and R. Zhang, J. Comput. Phys. **152**, 642 (1999).
[31] J. Glimm, J. W. Grove, and Y. Zhang, SIAM J. Sci. Comput. (USA) **24**, 208 (2002).
[32] J. Glimm, X. Li, R. Menikoff, D. Sharp, and Q. Zhang, Phys. Fluids A **2**, 2046 (1990).
[33] T. T. Clark, Phys. Fluids **15**, 2413 (2003).
[34] G. Dimonte and M. Schneider, Phys. Fluids **12**, 304 (2000).
[35] A. Banerjee and M. J. Andrews, Phys. Fluids **18**, 035107 (2006).
[36] K. O. Mikaelian, Physica D **36**, 343 (1989).
[37] M. B. Schneider, G. Dimonte, and B. Remington, Phys. Rev. Lett. **80**, 3507 (1998).
[38] D. Oron, L. Arazi, D. Kartoon, A. Rikanti, U. Alon, and D. Shvarts, Phys. Plasmas **8**, 2883 (2001).
[39] G. Dimonte, Phys. Rev. E **69**, 056305 (2004).
[40] G. Dimonte *et al.*, Phys. Fluids **16**, 1668 (2004).
[41] A. W. Cook, W. Cabot, and P. Miller, J. Fluid Mech. **511**, 333 (2004).
[42] P. Ramaprabhu, G. Dimonte, and M. J. Andrews, J. Fluid Mech. **536**, 285 (2005).
[43] P. Ramaprabhu, G. Dimonte, Y.-N. Young, A. C. Calder, and B. Fryxell, Phys. Rev. E **74**, 066308 (2006).
[44] D. L. Youngs, Phys. Fluids A **3**, 1312 (1991).
[45] Y.-N. Young, H. Tufo, A. Dubey, and R. Rosner, J. Fluid Mech. **447**, 377 (2001).
[46] R. D. Richtmyer, Commun. Pure Appl. Math. **13**, 297 (1960).